JOURNAL OF MATERIALS SCIENCE 28 (1993) 4003–4009

Relevance of free-surface temperature to thermal and kinetic factors in melt spinning

X. ZHANG, A. ATRENS
Department of Mining and Metallurgical Engineering, The University of Queensland, Queensland 4072, Australia

The relationship between the free-surface temperature history and the thermal and kinetic factors involved in melt spinning has been examined using a thermokinetic model for rapid solidification. Results show that the relationship is quite substantial. Measurement of the free surface temperature history can lead to the estimation of some of the factors involved which are otherwise very difficult to measure. Once these factors are determined, the real situation in rapid solidification can be modelled.

Nomenclature

A	Pre-exponential coefficient for the nucleation rate expression.
C_p	Specific heat with C_l and C_s representing that for liquid and solid, respectively.
D	The pre-basial constant for the crystal growth kinetic model.
δ	The thickness of the solidifying slab.
ΔG^*	Activation barrier for homogeneous nucleation.
$\Delta G'$	Gibbs free energy change for an atom jumping from liquid to solid.
γ	Atomic jump frequency.
h	Heat transfer coefficient.
I	Nucleation rate with I_s and I_t representing the steady state and transient nucleation rate, respectively.
k	Boltzmann's constant.
K	Heat conduction coefficient with K_l and K_s representing that for liquid and solid, respectively.
L	Latent heat.
n	The power index of the crystal growth kinetic model.
N^*	Number of atoms in the critical nucleus.
ρ	Density of the material with ρ_l and ρ_s representing that for liquid and solid, respectively.
t	Time coordinate.
T_i	Initial temperature of the cooling substrate.
T_2	Initial liquid temperature.
T_I	Interface temperature.
T_m	Melting point.
T_n	Nucleation temperature.
ΔT	Undercooling: $\Delta T = T_m - T_I$.
t_s	The time at the onset of solidification.
V	Interface velocity.
x	Space coordinate.

1. Introduction

Since the discovery of melt quenching by Duwez *et al.* [1] and the invention of the melt-spinning technique by Pond [2], a great deal of research effort has been directed at rapid solidification which has resulted in a rapid development in this area. Microstructural refinement, solubility extension and the formation of metastable phases are the main effects of melt quenching which offer approaches to improve the properties of materials. As an effort to understand the mechanism of melt quenching, mathematical modelling of rapid solidification processes has also attracted quite extensive attention [3–6]. Unfortunately, the lack of information regarding the melt–substrate heat-transfer coefficient, the nucleation temperature and the liquid–solid interface temperature during solidification have made the models more assumptive than realistic. These factors cannot be measured directly owing to the high rate of cooling in rapid solidification. What can be measured is the free-surface temperature, which has been done by several researchers [7–9] by high-speed infrared thermometry.

In our earlier paper [10], we presented a thermokinetic model for rapid solidification. The numerical results showed that the free surface temperature in melt spinning was influenced quite substantially by the thermal and kinetic factors involved. Here we examine further the relationship between the free-surface temperature and different thermal and kinetic factors in an attempt to find an approach to determine the uncertain thermal and kinetic factors by measuring the free-surface temperature–time profile using high-speed infrared thermometry.

2. The thermokinetic model

In our model [10], we considered melt spinning ideally as a thin slab of liquid metal of unit area at a

0022–2461

homogeneous initial temperature brought into contact suddenly with a flat cold substrate initially at a homogeneous low temperature and cooled down with such a large heat-transfer coefficient that cooling on the free surface and the perimeter can be neglected. The convective heat transfer due to fluid flow was neglected because the Prandtl number is very small for liquid metal, which is the ratio of the momentum diffusivity to the thermal diffusivity and is about 0.012 for copper at the melting point. In view of the composition homogeneity in rapidly solidified microstructure, the mass transfer owing to diffusion was also neglected in the model [10].

In order to solve the one-dimensional heat-transfer equations, the liquid–solid interface temperature must be known as a boundary condition. Under the circumstances of rapid solidification, the interface temperature is not known and may keep changing. This introduces an extra degree of freedom. Fortunately the interface temperature is related to the interface velocity by the crystal growth kinetics and the interface velocity is also determined by the thermal conditions near the interface which are governed by the heat-transfer equations. This inter-relationship makes it possible to couple the heat-transfer equations and the crystal growth kinetics to solve the whole problem. In our model [10], we first assumed the nucleation temperature, then used an iteration process to decide the interface temperature at each time step by the interface kinetics. At each time step, we first assume an appropriate starting estimate of the interface temperature, solve the heat-transfer equation and calculate the interface velocity. Then the calculated interface velocity is used to determine a new estimate of the interface temperature by the crystal growth kinetics. The new estimate of the interface temperature is then used as the boundary condition to solve the heat-transfer equation again and so on. This iteration process continues until the difference of the newly estimated interface temperature and the newly calculated interface temperature is smaller than the pre-set tolerance. For details of the algorithm, please refer to the earlier paper [10].

The crystal growth kinetics of some metals under large undercoolings has been studied by several researchers [11, 12] either by high-speed photography of the top surface of the melt, or by monitoring the temperature change during recalscence using infrared thermometry. Colligan and Bayles [11] measured the growth velocity of nickel at undercoolings between 20 and 200 K both by high-speed thermometry and high-speed photography of the top surface. Their results could well be fitted into a power law [11]: $V = 2.8 \times 10^{-3} \Delta T^{1.8}$ (m s^{-1}). Walker [12] measured the growth velocity of cobalt at large undercoolings. His result could also be fitted as a power law with a power index of 1.8, i.e. $V = 4.26 \times 10^{-3} \Delta T^{1.8}$ (m s^{-1}). Rosenberg and Winegard [13] measured the growth rate of tin dendrites at small undercoolings between 0.4 and 11 K. Their result could also be fitted [13] as a power law with a power index of 1.8, i.e. $V = 7.0 \times 10^{-3} \Delta T^{1.8}$ (m s^{-1}). It seems reasonable to assume a growth rate of power law $V = D\Delta T^n$ for copper under large undercoolings with $n = 1.8$ and D within the range from $D = 2.8 \times 10^{-3}$–7.0×10^{-3}. In the following calculation, we will assume a comparable growth power law for copper

$$V = 5.0 \times 10^{-3} \Delta T^{1.8} \text{ (m s}^{-1}\text{)} \quad (1)$$

unless the pre-basial constant and the power index are required to change for discussion of their effects. The maximum undercooling attainable for copper is 236 K [14]. We will assume an initial undercooling of 150 K unless specified otherwise.

3. Numerical results

Take the slab of metal to be copper, initially at T_2 K cooled down by a copper substrate at an initial temperature of T_1 K, the computed results using the model [10] are presented in the following section. The thermophysical properties of copper are listed in Table I.

3.1. The effect of the heat-transfer coefficient

The melt–substrate heat exchange can [6] be approximated as a heat-transfer coefficient h, which is the proportionality constant between the temperature drop across the interface and the resultant heat flux. This coefficient ranges from 10^4–10^7 W m^{-2} K^{-1} for melt spinning. It not only depends on the nature of the thermal contact between the melt and the substrate wheel, but also depends on the contact area which, in turn, is influenced by the melt–substrate wetting angle, cleanliness of the substrate surface and wheel surface speed. This coefficient has been estimated by Takeshita and Shingu [17] for the case of melt-spinning Ni–P glass ribbons using copper, steel and stainless steel substrate wheel by fitting the measured surface temperature with the calculated surface temperature of the glass ribbon with a cooling model where no solidification was involved. They found that the heat-transfer coefficient in the case of a copper substrate wheel ranged from 7.5×10^5 W m^{-2} K^{-1} for a wheel surface speed of 17 m s^{-1} to 1.3×10^6 W m^{-2} K^{-1} for

TABLE I Thermophysical properties of copper [15, 16]

	T_m (K)	L (kJ kg^{-1})	C_p (J kg^{-1} K^{-1})	K (W m^{-1} K^{-1})	ρ (kg m^{-3})
Cu (liquid)	1353.0	204.91	501.6	168.5	8047.0
Cu (solid)	–	–	397.1	350.0	8389.3
Cu (substrate)	–	–	397.1	392.0	8728.8

a wheel surface speed of 33 ms^{-1}. They also found that the contact area between the melt and the copper substrate was directly proportional to the wheel-surface speed.

We here choose three values of this important coefficient, i.e. $h = 8.0 \times 10^5$, 1.0×10^6, 2.0×10^6 W m^{-2} K^{-1}, to study its effects on the surface temperature when solidification is taken into account using our model [10]. Assuming a superheating of 120 K, an initial undercooling of 150 K and the crystal growth kinetic power law mentioned above with the initial melt temperature $T_2 = 1473$ K, the initial substrate temperature $T_1 = 303$ K and ribbon thickness $\delta = 30$ μm, the computed results of the free-surface temperature–time profile are shown in Fig. 1. The free-surface temperature–time profiles show a very steep cooling slope before the onset of solidification and then recalscence at the beginning of solidification to a relatively steady platform after some time as solidification proceeds and then a steep cooling slope after solidification finishes. The effect of this coefficient is very substantial. It not only affects the cooling rate of the pre-solidification and post-solidification cooling, but also influences the total solidification time and the temperature at the beginning of solidification. However, the temperature value at the platform after solidification has proceeded for some time is hardly influenced by this factor.

The substantial effect of the heat-transfer coefficient on the pre-solidification cooling rate can be used to determine the heat-transfer coefficient by fitting the measured pre-solidification cooling rate with the calculated pre-solidification cooling rates with different heat-transfer coefficients using the model [10]. The average cooling rates for the free surface before onset of solidification with different heat-transfer coefficients are listed in Table II.

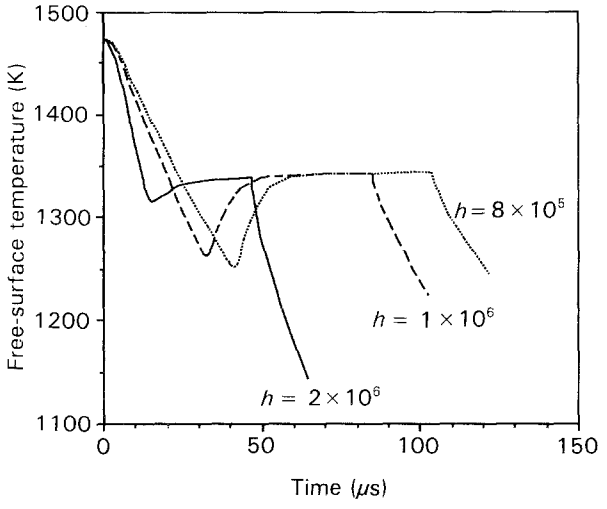

Figure 1 Free-surface temperature histories with different heat-transfer coefficients as indicated for a copper slab solidifying on a copper substrate. $\delta = 30$ μm, $T_1 = 303$ K, $T_2 = 1473$ K, $T_n = 1203$ K, $V = 5.0 \times 10^{-3} \Delta T^{1.8}$ ms^{-1}.

TABLE II Pre-solidification average cooling rate for different heat-transfer coefficients ($\delta = 30$ μm, $T_2 = 1473$ K, $T_1 = 303$ K, $T_n = 1203$ K, $V = 5.0 \times 10^{-3} \Delta T^{1.8}$ (ms^{-1}))

h($Wm^{-2}K^{-1}$)	Onset time, t_s(μs)	Average cooling rate (pre-solid.) (Ks^{-1})
8×10^5	39.7	6.8×10^6
1×10^6	30.9	8.8×10^6
2×10^6	12.9	2.1×10^7

3.2. The effect of the ribbon thickness

The ribbon formation and its final thickness was once a topic in melt-spinning modelling. Takeshita and Shingu [18] coupled the heat and momentum transport processes in melt spinning of $Fe_{40}Ni_{40}P_{14}B_6$ metallic glass and found that the ribbon-formation process is mainly momentum-transport controlled when the heat-transfer coefficient is not so large, and even when the heat-transfer coefficient is large, the momentum-transport mechanism still acts significantly through the dramatic decrease in viscosity. Their results showed a maximum momentum boundary-layer thickness at a certain value of the heat-transfer coefficient. Granasy [19] solved the partial differential equations of the boundary-layer theory taking into account the heat- and momentum-transport processes for the melt spinning of the same glass and found out that the thickness of the momentum boundary layer increases monotonically with increase in heat-transfer coefficient, which is quite different to Takeshita and Shingu's [18] result. Nevertheless, the momentum-transport mechanism is very important in determining the final thickness of the ribbon. From a point of view of the coupled heat- and momentum-transport controlled ribbon-formation process, the ribbon thickness will depend mainly on the heat-transfer coefficient and/or the substrate wheel-surface speed, the melt-jetting speed and the initial melt temperature. When other factors were kept constant, the measured ribbon thickness for amorphous $Fe_{40}Ni_{40}P_{14}B_6$ was related [20] to the substrate wheel-surface speed by $\delta = C V_w^{-0.8}$ where $C = 4.76 \times 10^{-4}$ $m^{1.8}s^{-0.8}$. Takeshita and Shingu's [18] result also showed that the momentum boundary-layer thickness inside the melt puddle is nearly the same along the melt-puddle length when the heat-transfer coefficient is large ($h = 1.68 \times 10^6$ $Wm^{-2}K^{-1}$) while it is quite uneven along the melt puddle when the heat-transfer coefficient is not so large ($h = 4.2 \times 10^5$ $Wm^{-2}K^{-1}$). We here assume an even thickness for the melt puddle in our calculation with heat-transfer coefficients larger than 8.0×10^5 $Wm^{-2}K^{-1}$.

In the following, we choose three different values of the melt-puddle thickness, i.e. $\delta = 30$, 40 and 50 μm, with a fixed heat-transfer coefficient $h = 2.0 \times 10^6$ $Wm^{-2}K^{-1}$, a fixed initial melt temperature $T_2 = 1473$ K and a fixed initial substrate temperature $T_1 = 303$ K, to see how the thickness of the ribbon influences the temperature history of the free surface. The computed results are shown in Fig. 2. The ribbon thickness not only affects the cooling rate before the onset of solidification but also the temperature at the beginning of solidification and the total solidification time.

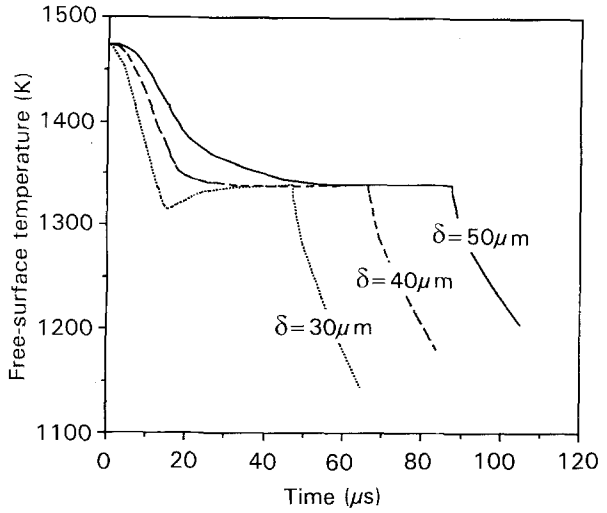

Figure 2 Free-surface temperature histories with different ribbon thickness as indicated for a copper slab solidifying on a copper substrate. $h = 2.0 \times 10^6$ W m^{-2} K^{-1}, $T_1 = 303$ K, $T_2 = 1473$ K, $T_n = 1203$ K, $V = 5.0 \times 10^{-3} \Delta T^{1.8}$ m s^{-1}.

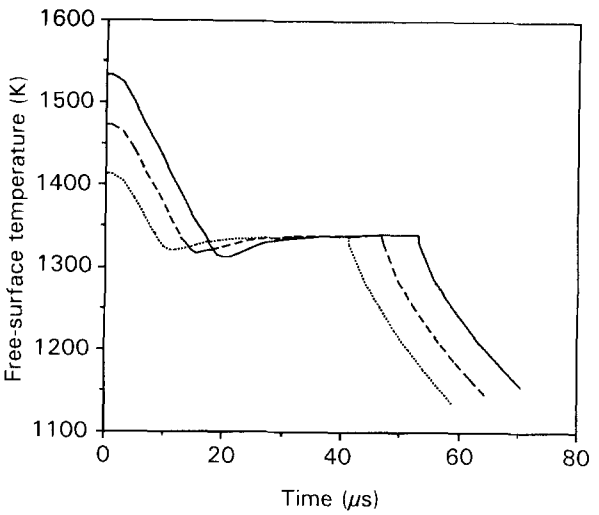

Figure 3 Free-surface temperature histories with different initial melt temperatures as indicated for a copper slab solidifying on a copper substrate. $h = 2.0 \times 10^6$ W m^{-2} K^{-1}, $\delta = 30$ μm, $T_1 = 303$ K, $T_n = 1203$ K, $V = 5.0 \times 10^{-3} \Delta T^{1.8}$ m s^{-1}. (···) $T_2 = 1413$ K, (– – –) $T_2 = 1473$ K, (——) $T_2 = 1533$ K.

The ribbon thickness can be measured accurately after melt spinning.

3.3. The effect of the initial melt temperature

Three different values of the initial temperature, i.e. $T_2 = 1413$, 1473 and 1533 K, were chosen to study its effect on the temperature history of the free surface with $h = 2.0 \times 10^6$ W m^{-2} K^{-1}, $T_1 = 303$ K and $\delta = 30$ μm. Results are shown in Fig. 3. It slightly influences the pre-solidification cooling rate and the total solidification time. This temperature can be monitored by using a thermocouple in melt spinning.

3.4. The effect of the initial substrate temperature

The computed free-surface temperature histories for three different values of the initial substrate temperature, i.e. $T_1 = 303$, 403 and 503 K, with the same initial melt temperature $T_2 = 1473$ K and $h = 2.0 \times 10^6$ W m^{-2} K^{-1} and $\delta = 30$ μm are shown in Fig. 4. The initial substrate temperature influences the pre-solidification and post-solidification cooling rate slightly. It also affects the surface temperature when the recalscence effect reaches the free surface. This temperature can be measured during melt spinning by using a contact-type thermocouple.

3.5. The effect of the nucleation temperature

In melt spinning, nucleation happens mostly on the melt–substrate contact surface as the microstructure of the melt-spun ribbons exhibit columnar grains growing from the contact side. Therefore, the nucleation temperature (or the initial undercooling) will depend mainly on the nucleation rate on the substrate. Two main factors are believed to influence the nucleation temperature in rapid solidification: one is the

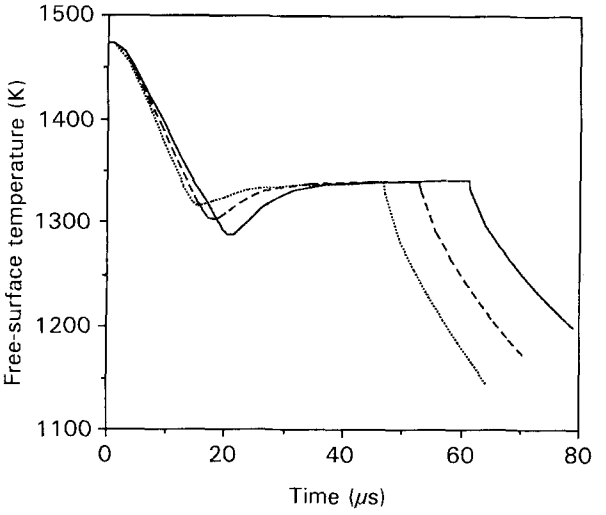

Figure 4 Free-surface temperature histories with different initial substrate temperatures as indicated for a copper slab solidifying on a copper substrate. $h = 2.0 \times 10^6$ W m^{-2} K^{-1}, $\delta = 30$ μm, $T_2 = 1473$ K, $T_n = 1203$ K, $V = 5.0 \times 10^{-3} \Delta T^{1.8}$ m s^{-1}. (···) $T_1 = 303$ K, (– – –) $T_1 = 403$ K, (——) $T_1 = 503$ K.

heterogeneous nucleation site and the other is the cooling rate, as melt subdivision (removal of heterogeneous sites) can result in large undercoolings and melt spinning can also produce large undercoolings which have been demonstrated by the formation of metastable phases. In calculating the nucleation rate for melt spinning, the nucleation rate expression should be carefully chosen to account for the heterogeneous nucleation situation under continuous cooling with a high cooling rate. Clyne [6] used the classical nucleation-rate expression and a summation process to define the onset of solidification in splat cooling. His result showed that the initial undercooling mainly depended on the melt–substrate contact angle and was relatively insensitive to the cooling rate. The latter point made it very difficult to explain how large undercooling is reached in splat cooling.

This was due to the use of the steady-state nucleation rate which overestimates the nucleation rate in splat cooling where transient behaviour should be considered.

The classical heterogeneous nucleation rate can be expressed [21] as

$$I = A \exp[-\Delta G f(\theta)/kT] \quad (2)$$

where ΔG^* is the activation barrier for homogeneous nucleation, k is Boltzmann's constant, T is the absolute temperature for nucleation, A is the pre-exponential coefficient of the order of 10^{27} cm^{-2}s^{-1} and is proportional to the number of liquid atoms in contact with unit area of the catalystic surface as well as the jump frequency of the atoms, and $f(\theta)$ is a contact angle factor. For nuclei having the form of a spherical sector on a planar catalystic site, this factor can be represented as

$$f(\theta) = (2 - 3\cos\theta + \cos^3\theta)/4 \quad (3)$$

with θ as the contact angle between the nucleus and the catalystic site. Equation 2 is for steady-state heterogeneous nucleation which assumes that the equilibrium cluster distribution exists before onset of nucleation. It has been shown [22] that it will take some time to reach this steady-state nucleation rate if no cluster distribution exists at the start of nucleation. This time lag could be of significant importance in the production of metastable phases in rapid solidification. The transient nucleation rate for isothermal homogeneous nucleation can be expressed [22] as

$$I_t = I^s[1 + 2C \sum_{m=1}^{\infty} (-1)^m \exp(-m^2 t/\tau)] \quad (4)$$

where I^s is the steady-state nucleation rate, I_t is the transient nucleation rate at time t, and τ can be represented [22] as

$$\tau = -\frac{6kTN^{*1/3}}{\pi^2 \gamma \Delta G'} \quad (5)$$

where N^* is the number of atoms in the critical nucleus; γ is the atomic jump frequency and $\Delta G'$ is the Gibb's free energy change for an atom jumping from the initial phase to the new phase. $C = 1$ if no cluster distribution exists at the start of nucleation. If the system is pre-annealed at temperature T' before it is brought to T for nucleation, C should be expressed [22] as

$$C = 1 - (\Delta q/Z)\exp(-N^*\Delta q) \quad (6)$$

with

$$Z = [-\Delta G'/(6\pi kTN^*)]^{1/2} \quad (7)$$

and

$$\Delta q = -\{[-\Delta G'(0) - \tfrac{3}{2}\Delta G'(T)]/k\}(1/T - 1/T') \quad (8)$$

For a first approximation, I^s in Equation 4 can be substituted by the steady-state heterogeneous nucleation rate, i.e. Equation 2, with correspondent parameters adjusted for a heterogeneous situation to give a nucleation-rate expression for transient isothermal heterogeneous nucleation. This can be used in Clyne's summation process [6] to define the onset of nucleation to give an approximation of the nucleation temperature in melt spinning. For more exact calculation, analytical expression for or numerical treatment of the transient heterogeneous nucleation rate under rapid cooling conditions needs to be developed. However, there is still uncertainty in the estimation of the atomic jump frequency, γ, even when this is done.

On the other hand, it may be possible to determine the nucleation temperature by fitting the measured surface temperature history with the calculated surface temperature histories using different nucleation temperatures in the model, if the variation in nucleation temperature can cause substantial change in the free-surface temperature history. Bearing this in mind, we here choose three different nucleation temperatures, i.e. T_n = 1173, 1223 and 1273 K, to see how the free-surface temperature history is influenced with the growth kinetics mentioned above and $h = 2.0 \times 10^6$ W m^{-2} K^{-1}, $\delta = 30$ μm, $T_1 = 303$ K and $T_2 = 1473$ K. The results computed by the model [10] are shown in Fig. 5. The effect is mainly in the beginning of solidification. For $T_n = 1173$ K, the free-surface temperature continues to decrease with nearly the same cooling rate until the lowest temperature $T = 1282.2$ K at $t = 17.6$ μs and then increases quickly to the platform temperature of $T = 1338$ K. For $T_n = 1223$ K, the free-surface temperature continues to decrease with nearly the same cooling rate until $T = 1343.1$ K at $t = 12.5$ μs, and then decreases very slowly to the lowest temperature $T = 1334.96$ K at $t = 18$ μs and then increases very slowly to the platform temperature $T = 1338$ K. For $T_n = 1273$ K, the free-surface temperature continues to decrease with nearly the same cooling rate until $T = 1421.1$ K at $t = 6.6$ μs and then decreases with a slower and slower rate to the platform temperature $T = 1338$ K. It is possible to estimate the nucleation temperature through the free-surface temperature measurement if these differences between $t = 6.5$ μs and $t = 25$ μs can be detected.

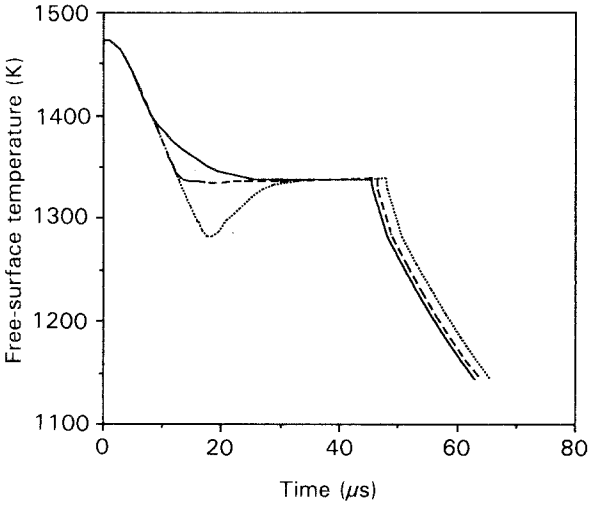

Figure 5 Free-surface temperature histories with different nucleation temperatures as indicated for a copper slab solidifying on a copper substrate. $h = 2.0 \times 10^6$ Wm^{-2}K^{-1}, $\delta = 30$ μm, $T_1 = 303$ K, $T_2 = 1473$ K, $V = 5.0 \times 10^{-3}\Delta T^{1.8}$ ms^{-1}. (···) $T_n = 1173$ K, (– – –) $T_n = 1223$ K, (———) $T_n = 1273$ K.

3.6. The effect of the crystal growth kinetics

Recent atomistic calculation by Monte Carlo simulation of crystal growth showed [23] that the crystal growth rate is directly proportional to the undercooling when the undercooling is small while the growth rate at large undercoolings can be fitted over a limited region as a power law $V = D\Delta T^n$ with n increasing progressively as undercooling increases. Experimental measurement of the growth rate at large undercoolings has also been conducted [11, 12]. Results showed a power law $V = D\Delta T^n$ with $n \approx 1.8$. We have chosen Equation 1 as the growth kinetics in all the calculations above.

Here we will allow the growth power law to change to see how the free-surface temperature is affected. Fig. 6 shows the free-surface temperature histories for different crystal growth power laws with different power indexes and a fixed pre-basial constant $D = 5.0 \times 10^{-3}$. Fig. 7 shows the free-surface temperature histories for different crystal growth power laws with different pre-basial constants and a fixed power index $n = 1.8$. All other factors were fixed at the calculation as follows: $h = 2.0 \times 10^6\ \mathrm{W\,m^{-2}\,K^{-1}}$, $\delta = 30\ \mu\mathrm{m}$, $T_2 = 1473\ \mathrm{K}$, $T_1 = 303\ \mathrm{K}$, $T_n = 1203\ \mathrm{K}$.

It can be seen that the effect of the power index and the pre-basial constant is mainly on the absolute temperature value after the beginning of solidification, especially the temperature value at the platform, and the total solidification time. The bigger the power index and/or the pre-basial constant, the larger the free-surface temperature during solidification and the shorter the total solidification time. The effect of the former (Fig. 6) is more significant than that of the latter (Fig. 7). It is also noted that the power index also influences the slope of the curve (Fig. 6), i.e. the time differential of the temperature, after the commencement of solidification.

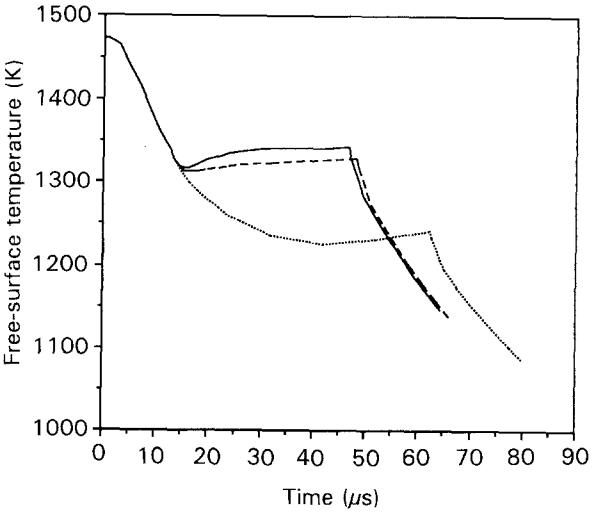

Figure 6 Free-surface temperature histories with different power indexes for the crystal growth kinetic law as indicated for a copper slab solidifying on a copper substrate. $h = 2.0 \times 10^6\ \mathrm{W\,m^{-2}\,K^{-1}}$, $\delta = 30\ \mu\mathrm{m}$, $T_1 = 303\ \mathrm{K}$, $T_2 = 1473\ \mathrm{K}$, $T_n = 1203\ \mathrm{K}$, $V = 5.0 \times 10^{-3}\,\Delta T_n\,\mathrm{m\,s^{-1}}$. (···) $n = 1.0$, (– – –) $n = 1.5$, (———) $n = 2.0$.

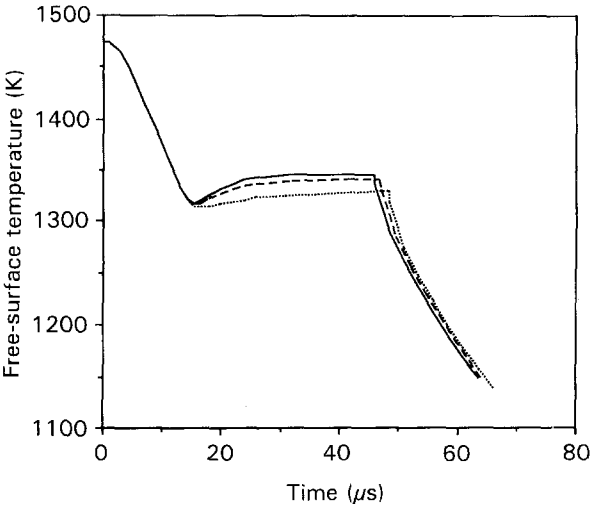

Figure 7 Free-surface temperature histories with different pre-basial constants for the crystal growth kinetic law as indicated for a copper slab solidifying on a copper substrate. $h = 2.0 \times 10^6\ \mathrm{W\,m^{-2}\,K^{-1}}$, $\delta = 30\ \mu\mathrm{m}$, $T_1 = 303\ \mathrm{K}$, $T_2 = 1473\ \mathrm{K}$, $T_n = 1203\ \mathrm{K}$, $V = D\,\Delta T^{1.8}\,\mathrm{m\,s^{-1}}$. (···) $D = 2.0 \times 10^{-3}$, (– – –) $D = 7.0 \times 10^{-3}$, (———) $D = 2.0 \times 10^{-2}$.

4. Discussion

4.1. Determination of the different factors

The initial melt and substrate temperatures can be measured directly at the start of the melt-spinning process. The thickness of the ribbon can be measured after the melt-spinning process. If a sensible curve of the free-surface temperature history similar to the calculated one can be obtained by infrared thermometry during the melt-spinning process, the heat-transfer coefficient can first be solely decided by the average slope of the pre-solidification cooling curve. The shape or the depth of the valley in the beginning of solidification can lead to the estimation of the nucleation temperature. The absolute temperature value at the platform after solidification proceeds for some time and the slope of the curve leading to the platform can give an estimation of the crystal growth kinetics.

4.2. Free-surface temperature measurement

It has been shown [18] that the momentum boundary-layer thickness is nearly the same along the melt-puddle length if the heat-transfer coefficient is large enough (around $1.68 \times 10^6\ \mathrm{W\,m^{-2}\,K^{-1}}$). This means that the thickness of the melt is nearly the same anywhere along the puddle length. This makes it possible to measure the free-surface temperature history by setting several sensors along the puddle length at certain intervals. It has also been shown [17] that the heat-transfer coefficient exhibited a maximum $h \approx 1.3 \times 10^6\ \mathrm{W\,m^{-2}\,K^{-1}}$ at a wheel-surface speed of $V_w \approx 33\ \mathrm{m\,s^{-1}}$ and then decreased with increasing wheel-surface speed for melt-spinning Ni–P glass using a copper substrate wheel. Assuming that a heat-transfer coefficient of about $1.0 \times 10^6\ \mathrm{W\,m^{-2}\,K^{-1}}$ corresponds to a wheel (copper) surface speed of $V_w = 60\ \mathrm{m\,s^{-1}}$ and the thickness of the resulting ribbon is 30 μm, the melt-puddle length will be about 6 mm because the solidification finishes at about 100 μs

(Fig. 1). Arranging the measuring setting at 1 mm intervals with the measuring spots 0.5 mm wide, which corresponds to a time lapse of about 17 and 8 μs, respectively, the temperature variation inside the measuring spot is of the order of 10 K, which represents a reasonably acceptable error for the temperature of the spots, and the time interval between two measuring spots is about 17 μs which is just short enough to give a sensible account for the valley in the beginning of solidification. These measuring settings require a data acquisition response time of not more than 10 μs and a channel switching time of not more than 17 μs. A response time of 6 μs has been achieved for infrared thermometry [24]. If these requirements can be satisfied, it seems possible to measure one or two temperatures before solidification begins and to measure three to four temperatures during solidification with one or two temperatures in the valley in the beginning of solidification. These data can lead to a sensible estimation of the factors mentioned above.

If each channel has its own data acquisition system with a response time of 10 μs and the measuring spots are allowed to move along the wheel surface in the same direction as the wheel at a lower speed, say $10\,m\,s^{-1}$, then around 30 data points covering the 6 mm length of the melt puddle can be obtained during a 100 μs run for a total of five channels. In the first run the substrate wheel temperature is the same everywhere, all points of the ribbon are spun under the same conditions and thus are identical, then the 30 data points can be converted to represent those for one point travelling across the 6 mm long puddle. Thus the smallest time lapse between two measuring spots is reduced to around $[10(\mu s)\,10(m\,s^{-1})/60(m\,s^{-1}) \approx 1.7\,(\mu s)$. This represents an equivalent response time of less than 2 μs. Therefore, a detailed account of the surface temperature can be obtained if such measurement is successful. The problem is how to reduce the width of the measuring spot with strong enough radiation for the sensing. A rectangular measuring spot will be preferable.

5. Conclusions

1. The larger the heat-transfer coefficient, the higher is the pre-solidification cooling rate for the free surface. This makes it possible for the heat-transfer coefficient to be determined through the average pre-solidification cooling rate by measurement of one or two temperatures before solidification starts.

2. Different nucleation temperatures cause different cooling behaviour for the free surface in the beginning of solidification. Large initial undercooling results in a deep valley in the beginning of solidification for the temperature–time profile of the free surface, ambient initial undercooling corresponds to a flatter temperature–time profile for the free surface during solidification, while small initial undercooling leads to a down-hill shape curve in the beginning of solidification for the free-surface temperature–time profile. These differences can lead to the estimation of the nucleation temperature in melt spinning by fitting the measured features of the free-surface temperature–time profile with the calculated ones with different nucleation temperatures.

3. The bigger the power index and/or the pre-basial constant for the crystal growth power kinetic law, the larger is the free-surface temperature during rapid solidification. This may lead to the estimation of the growth power kinetic law by matching the measured with calculated free-surface temperature–time profile using the model.

Acknowledgement

This project was supported by the Australian Research Council.

References

1. P. DUWEZ, R. H. WILLENS and W. KLEMENT JR, *J. Appl. Phys.* **31** (1960) 1136.
2. R. B. POND, US Pat. 2825108, 4 March 1958.
3. Z. SUN and H. A. DAVIES, *Mater. Sci. Engng* **98** (1988) 71.
4. G. X. WANG and E. F. MATTHYS, *Int. J. Rapid Solid.* **6** (1991) 141.
5. K. TAKESHITA and P. H. SHINGU, *Trans. Jpn. Inst. Metals* **24** (1983) 293.
6. T. W. CLYNE, *Metall. Trans.* **15B** (1984) 369.
7. G. STEPHANI, H. MUHLBACH, H. FIEDLER and G. RICHTER, *Mater. Sci. Engng* **98** (1988) 29.
8. P. CREMER and J. BIGOT, *ibid.* **98** (1988) 95.
9. E. VOGT, *Int. J. Rapid Solid.* **3** (1987) 131.
10. X. ZHANG and A. ATRENS, *ibid.*, **7** (1992) 83.
11. G. A. COLLIGAN and B. J. BAYLES, *Acta Metall.* **10** (1962) 895.
12. J. L. WALKER, unpublished results presented in B. Chalmers, "Principle of Solidification", (Wiley, 1962) p. 115.
13. A. ROSENBERG and W. C. WINEGARD, *Acta Metall.* **2** (1954) 342.
14. J. H. HOLLOMON and D. TURNBULL, *Prog. Met. Phys.* **4** (1953) 333.
15. C. J. SMITHELLS, "Metals References Book", 5th Edn (Butterworths, 1976).
16. Y. S. TOULOUKIAN and C.Y. HO, "Thermophysical Properties of Matter", TPRC Data Series, Vols 1 and 4 (Plenum, USA, 1970).
17. K. TAKESHITA and P. H. SHINGU, *Trans. Jpn. Inst. Metals* **27** (1986) 454.
18. *Idem, ibid.* **24** (1983) 529.
19. L. GRANASY, *ibid.* **27** (1986) 51.
20. H. HILLMANN and H. R. HILLZINGER, "Rapidly Quenched Metals III", Vol. 1 (The Metal Society, 1978) p. 22.
21. J. H. PEREPEZKO in "Science and Technology of Undercooled Melt", edited by P. R. Sahm, H. Jones and C. M. Adams (Martinus Nijhoff, 1986) p. 29.
22. K. F. KELTON, A. L. GREER and C. V. THOMPSON, *J. Chem. Phys.* **79** (1983) 6261.
23. K. A. JACKSON, *Mater. Sci. Engng* **65** (1984) 7.
24. T. J. PICCONE, Y. WU, Y. SHIOHARA and M. C. FLEMINGS, *Metall. Trans.* **18A** (1987) 925.

Received 16 January
and accepted 20 November 1992